ADVANCED QUANTUM TECHNOLOGIES
www.advquantumtech.com

Free-Space Quantum Key Distribution with Single Photons from Defects in Hexagonal Boron Nitride

*Çağlar Samaner, Serkan Paçal, Görkem Mutlu, Kıvanç Uyanık, and Serkan Ateş**

Efficient single photon generation is an important requirement for several practical applications in quantum technologies, including quantum cryptography. A proof-of-concept demonstration of free-space quantum key distribution (QKD) is presented with single photons generated from an isolated defect in hexagonal boron nitride (hBN). The bright source operating at room temperature is integrated into a QKD system based on B92 protocol and a sifted key rate of 238 bps with a quantum bit error rate of 8.95% are achieved at 1 MHz clock rate. The effect of temporal filtering of detected photons on the performance of QKD parameters is also studied. It is believed that these results will stimulate the research on optically active defects in hBN as well as other 2D-based quantum emitters and their applications within quantum information technologies including practical QKD systems.

1. Introduction

Quantum key distribution (QKD) is one of the most developed applications within quantum information technologies. The first proposed QKD protocol, known as BB84,[1] relies on the polarization of photons for encoding information. Among several approaches, using weak coherent pulses as the light source provides a practical approach to realize a QKD system, although it is inefficient[2] and has possible security weaknesses under photon number splitting attacks (PNS).[3] These issues are addressed by using decoy states,[4,5] which are also implemented in practical QKD systems using integrated photonic and electronic circuits.[6,7] However, ultimate security and long-distance operation still require true single photon sources (SPSs) with high efficiency. To date, several SPSs have been used in different QKD demonstrations, such as optically[8–11] or electrically[12,13] excited semiconductor quantum dots (QDs) and color centers in diamond.[14–16] Although semiconductor QDs have the advantage of easier integration with cavity-based systems and electrical operation, they require cryogenic temperatures for efficient operation. Alternatively, color centers in diamond nanocrystals generate bright emission at room temperature and they can be implemented in nanophotonic structures for applications in integrated photonic technologies.[17] In addition to these SPSs, a recent study shows that single dibenzoterrylene molecules embedded in nano-crystals are also good candidates for QKD systems due to their high efficiency at room temperature.[18] There is also a growing interest on entanglement-based QKD systems[19,20] that mostly use nonlinear crystals[21] or semiconductor quantum dots[22–24] for efficient generation of entangled photon pairs.

Despite all the efforts on the above-mentioned SPSs, interest has grown for quantum emitters in 2D materials, including transition metal dichalcogenides (TMDCs) and defects in hexagonal boron nitride (hBN).[25] TMDC materials show direct bandgap structure when they are in monolayer form and provide bright single photon emission from trapped excitons. However, similar to semiconductor QDs, single photon emission from these structures require cryogenic temperatures. On the other hand, hBN is known as a 2D indirect bandgap semiconductor.[26] Thanks to its wide bandgap ($\approx$ 6 eV), hBN hosts several types of optically active defects[27] that generate efficient single photon emission from cryogenic temperatures[28–31] up to 800 K[32] over a wide spectral range from UV[33] to NIR.[34] The fact that hBN hosts bright and optically stable emitters, in addition to its scalability owing to its 2D nature, makes it a great candidate for several room temperature applications within the quantum technologies, for example, quantum random number generation and nanoscale optical thermometry.[25,35–39]

Here, we present, to the best of our knowledge, the first proof-of-concept demonstration of B92-based QKD[40] with single photons generated from an isolated defect in hBN. Brightness and purity of zero-phonon line (ZPL) emission of the defect are characterized under pulse excitation conditions at room temperature. The pre-characterized emission is used in a QKD system where the polarization encoding is realized at 1 MHz clock rate. Sifted key rate (SKR) and quantum bit error rate (QBER) are also optimized via temporal filtering of the detected photons. Finally, we have performed simulations to understand how the secret key rate (the key rate after post-processing, i.e., error correction and privacy amplification) depends on the channel loss to compare the efficiency of studied hBN defect to the alternative single photon emitters. We anticipate that our results will stimulate the

Ç. Samaner, S. Paçal, G. Mutlu, S. Ateş
Department of Physics
İzmir Institute of Technology
İzmir 35430, Turkey
E-mail: serkanates@iyte.edu.tr
K. Uyanık
Department of Physics
Gazi University
Ankara 06500, Turkey

The ORCID identification number(s) for the author(s) of this article can be found under https://doi.org/10.1002/qute.202200059

DOI: 10.1002/qute.202200059

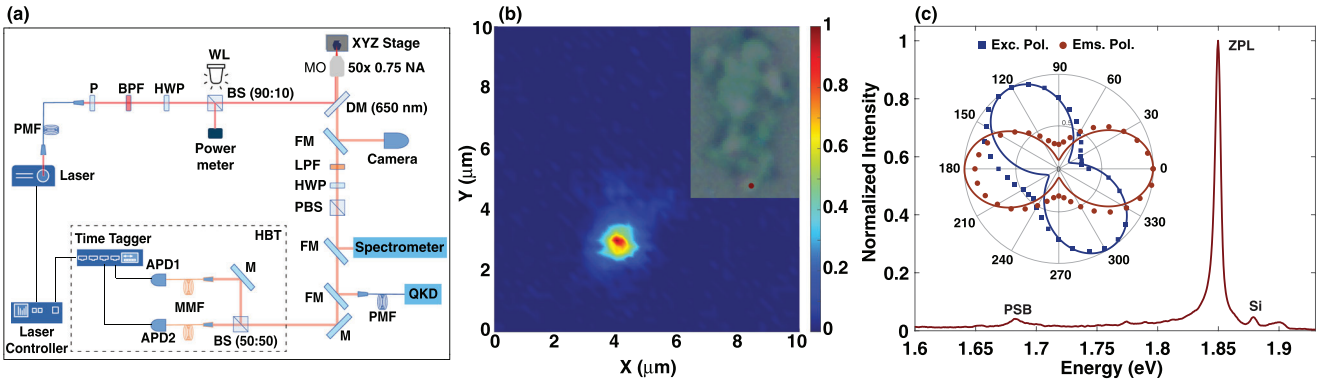

Figure 1. a) Schematic representation of confocal micro-PL setup that is used to characterize the optical properties of single defects in hBN. Collected emission is spectrally analyzed by a spectrometer, and its single photon nature is measured with an HBT interferometer. Spectrally filtered and polarized single photon emission is guided to the QKD system via a polarization maintaining single mode fiber. b) PL map of a bulk hBN with a bright localized emission. Inset shows the optical image of the studied hBN structure. c) PL spectrum of the isolated defect taken under 1 MHz repetition rate shows the ZPL and PSB emission of the defect as well as the Raman scattering from silicon substrate. The inset shows the excitation (square) and emission (circle) polarization dependent intensity of ZPL emission.

implementation of quantum emitters in hBN for various applications in quantum technologies.

2. Optical Characterization of hBN–Based Single Photon Source

Schematic of the experimental setup that is used to characterize the optical properties of defects in hBN is given in **Figure 1**a. A 637 nm pulsed laser is used for excitation that passes through a polarizer and a half-wave plate (HWP) for polarization manipulation. A high numerical aperture microscope objective (NA= 0.75) is used to focus the laser light and to collect the emission from the sample, which is placed on a high-resolution XYZ stage for precise positioning and for the scanning purposes. A 650 nm long pass dichroic mirror is used to direct the laser light onto the sample and transmit the emission to the detection port efficiently. An additional 650 nm long pass filter is placed on the detection for further filtering of the laser light. Collected emission is then passed through a HWP and a polarizing beamsplitter (PBS) for polarization analysis and directed either to a spectrometer for spectral analysis or to a Hanbury–Brown and Twiss (HBT) interferometer for photon correlation measurements. The interferometer contains a 50/50 beamsplitter and two single-photon detectors (ID120, ID Quantique). Finally, pre-characterized emission is guided to the QKD setup by a polarization-maintaining single-mode fiber, which also acts as a pinhole to spatially filter the ZPL emission. Details of the QKD setup are described below.

Multilayer hBN flakes are obtained from a solution (Graphene Supermarket) and drop-casted on a SiO2/Si substrate. All data presented in this work are obtained from a single defect in hBN operating at room temperature. A photoluminescence map of the investigated structure and its optical image are shown in Figure 1b. The localized bright emission observed in the map is due to an isolated defect with the emission spectrum (recorded under 1 MHz laser repetition rate) given in Figure 1c. The defect has a sharp zero-phonon line (ZPL) emission at 1.848 eV (671 nm) with a characteristic optical phonon sideband (PSB) at 1.683 eV (736 nm). Energy difference between the ZPL and the PSB is about 165 meV that matches perfectly with the energy of the high-energy Raman active phonon mode of the host hBN. As observed, the ZPL emission from the defect dominates strongly in the whole spectrum, indicating a large Debye–Waller factor.[41] In this type of hBN flakes, it is quite challenging to identify the origin of defects from ZPL energy due to uncontrolled natural strain around the defect, which can shift the ZPL energy quite strongly.[42] The inset of Figure 1c shows the absorption and emission polarization of the ZPL with a high degree of visibility (≈ 78%) as expected for a single dipole. The observed misalignment between the measured polarization patterns is reported before, and it is mainly attributed to an indirect excitation process for defects in hBN.[43]

Besides the strong linear polarization of ZPL emission observed here, its brightness is another important property for practical QKD systems. To quantify the brightness of the same emitter, excitation power dependent saturation measurement is performed on the spectrally filtered ZPL emission (FB670-10, Thorlabs) with a fiber-coupled single photon detector. **Figure 2**a shows the result of this measurement taken under 40 MHz repetition rate of the laser and the solid line represents the fit using $R = (R_\infty * P)/(P + P_{sat})$ function obtained from three-level model of defects in hBN.[28] Here, R_∞ and P_{sat} are the maximum emission rate and the excitation power at which the intensity saturates, respectively. Although the highest measured count rate is 150 kHz under maximum available excitation power, fit results indicate a maximum achievable emission rate of 495 kHz under stronger excitation conditions, which is not observed due to limited power of the available excitation laser. Considering all performances of the components used for this measurement (detector efficiency, coupling into multimode fiber, efficiency of bandpass filter, transmission of dichroic mirror and efficiency of several optics over the path), a count rate of 1.2 MHz is achieved after the microscope objective. This corresponds to a 3% collection efficiency under the highest excitation power of the laser at 40 MHz repetition rate, which reaches up to 10% for the maximum emission rate of 495 kHz, considering a 100% quantum yield of the emitter. However, direct measurement of quantum yield for similar types of defects in hBN were reported to be about 40%,[44]

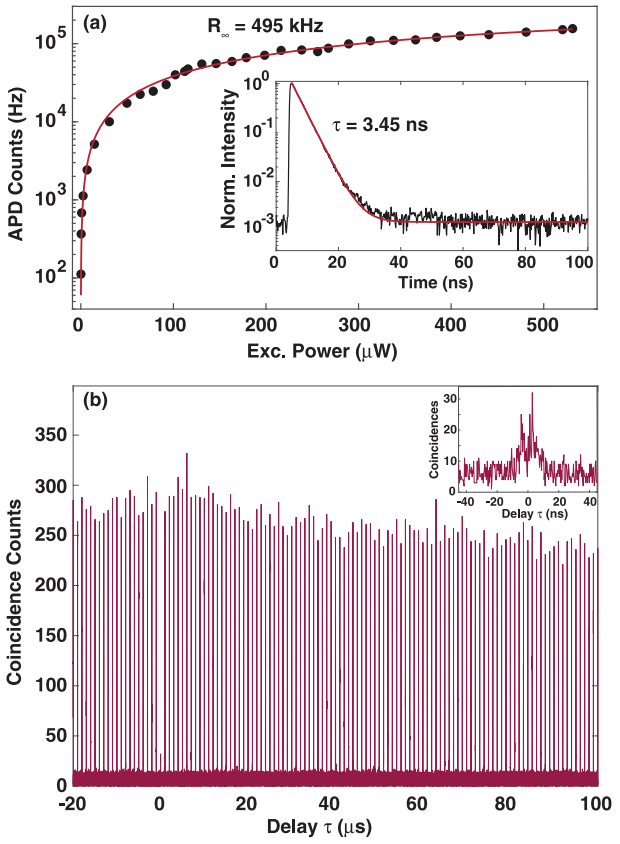

Figure 2. a) Excitation power dependence of ZPL emission (spectrally filtered) measured with an APD under 40 MHz repetition rate. Inset: Time-resolved PL of the defect with a decay time of 3.45 ns. b) Second-order photon correlation measurement of the same emitter taken under 1 MHz repetition rate. The anti-bunching value is estimated as $g^{(2)}(0) = 0.12 \pm 0.03$. The inset shows the magnified zero time delay region for clarity.

indicating even higher collection efficiencies could be achieved potentially. Collection efficiency of the ZPL emission can be further improved by either using solid-immersion lenses[45] or coupling the emitters to nano-photonic[46] or plasmonic structures.[47]

In addition to the saturation, the dynamics of the ZPL emission is measured using time-correlated single photon counting method. Inset of Figure 2a shows the result of such an experiment under 10 MHz excitation rate. A single exponential decay with a lifetime of 3.45 ± 0.05 ns is observed for the studied defect.[28] We also examined the purity of the emitted photons by measuring the second-order photon correlation function, $g^2(\tau)$, using the HBT interferometer. The result of such an experiment performed on the spectrally filtered ZPL emission (Thorlabs FL670-10) is shown in Figure 2b. While the number of coincidences decrease exponentially over long time delays as expected for a three-level emitter, a clear anti-bunching is observed at zero time delay with a value of $g^2(0) = 0.12 \pm 0.02$. This experiment is performed under 1 MHz excitation rate under full available excitation power (≈ half of the saturation), which is also used for the demonstration of QKD with the same emitter. Finally, the linearly polarized single photon emission from the defect is coupled to a polarization-maintaining fiber for the demonstration of QKD.

3. Demonstration of Quantum Key Distribution

In this work, a B92-based protocol is implemented due to its simplicity and the availability of the equipment at the expense of lower key rate efficiency compared to the BB84 protocol. In the B92 protocol, Alice randomly prepares the photon polarizations in any two non-orthogonal states, for example, 90 degree and +45 degree, corresponding to a bit value of 0 and 1, respectively. Bob performs random measurements on two orthogonal polarizations with respect to the prepared states (0 degree and −45 degree) to distinguish the encoded photons. A measurement in the 0 degree corresponds to a bit value of 1 while a measurement of −45 degree corresponds to a bit value of 0. For key sifting, Bob shares with Alice the time of each measurement event without actual measurement result to form the final key, which is then post-processed to create the final secret key. The schematic of the free-space QKD system is shown in **Figure 3**. The transmitter (Alice) uses a pulse generator to trigger the excitation laser (inside the single photon source box) and to feed the high voltage amplifier (New Focus HVA 3211) that drives the broadband electro-optic amplitude modulator (EOM, New Focus 4102) utilized for polarization encoding of single photons. Due to the capacity of the high-voltage amplifier, the maximum repetition rate of the entire system is limited to 1 MHz. Single photon emission is passed through a half-wave plate and a polarizer to set vertical polarization input with a high extinction ratio before entering the EOM. In our implementation of the protocol, vertical and +45 degree polarizations are encoded on single photons, which are obtained by driving the EOM with 0 and 95 V, respectively, and using a quarter-wave plate (QWP) behind the EOM to convert the circular polarization output to linear polarization. In this experiment, a periodic encoding of polarizations (010101...) is used for a proof-of-concept demonstration.[13] The receiver (Bob) employs a non-polarizing 50:50 BS to choose a random measurement basis, and two PBSs and a HWP for polarization selection. In addition, two fiber-coupled APDs are attached to the output ports of each PBS for detection of single photons. Finally, a time tagging module is used both to record the time of measurement events from each APD and to synchronize Alice and Bob via the common trigger signal generated by the pulse generator on the Alice side.

The demonstration of QKD is performed under 1 MHz repetition rate and at the highest achievable power of the excitation source (not enough to saturate the defect as discussed before). A total count rate of 30 kHz after the microscope objective and 7.8 kHz at the input of Alice are obtained under this excitation condition. The count rate is further degraded to 400 Hz on each APD (on top of ≈1.5 kHz dark counts) because of all the performances of the QKD system in use (i.e., optics, EOM transmission, detection efficiency of APDs, fiber couplings, and the 25% efficiency of the protocol), which therefore indicates a total efficiency of the QKD system after the first lens to be about 2.67%.

Figure 4a,b shows the histograms of relative time differences between a laser trigger and APD detection events that are acquired for a 2.5 s-long run of QKD experiment. Since the lifetime of the emitter is 3.45 ns, main contribution to the observed 148 ns delay in the histograms comes from the electronics of the system. The distribution of detection events around this delay gives a bound for SKR and QBER analysis. Here, the width of the distribution is used as temporal filtering to eliminate the

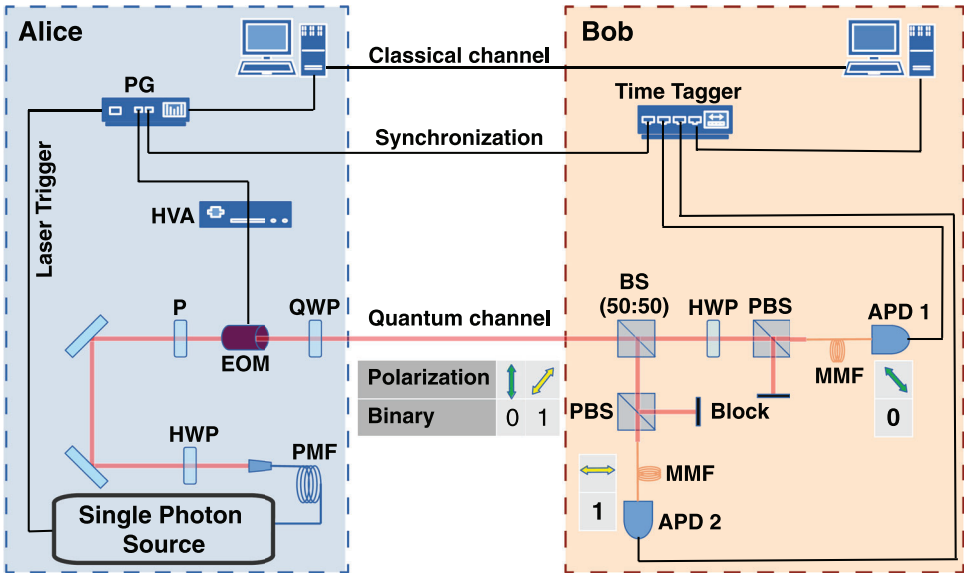

Figure 3. Experimental setup of B92-based free-space QKD system. Alice Side: One channel of the pulse generator drives the single photon source system at 1 MHz repetition rate and simultaneously sends the reconciliation signal to the time tagging module, which is used for synchronization of the system. The other channel sends a periodic pattern signal to the EOM. The modulator controls the polarization of the photons to be vertical (0) or +45 degree (1) according to the incoming signal. Bob Side: A 50/50 beam splitter (BS) randomly directs the incoming photons to either APD1 or APD2 for polarization analysis. APD1 detects only if the photon has -45 (0) polarization while APD2 detects if it has H (1) polarization and the time of each detection event is recorded by time tagging module for reconciliation process.

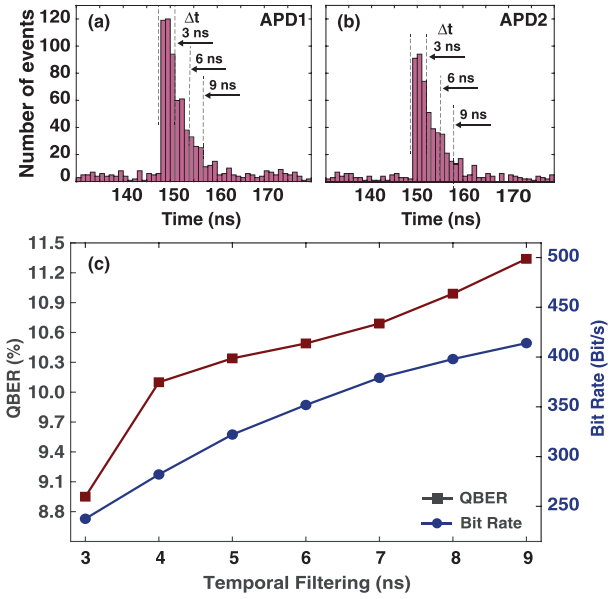

Figure 4. a,b) Histograms of relative time differences between laser trigger and detection on APDs. Each bin shows the total counts in 1 ns time interval for a total of 2.5 second of QKD demonstration. c) Change of QBER and bit rate as a function of temporal filtering.

effect of random dark counts of APDs outside of this bound and to increase the signal-to-noise ratio. However, there is a trade-off between key rate and QBER as a function of temporal filtering, Δt, as shown in Figure 4c. As observed, decreasing the Δt reduces the QBER due to the limited contribution of dark counts. Considering the events in the 3 and 9 ns filtering durations, QBER and SKR are measured as $QBER_{3ns} = 8.95\%$, $SKR_{3ns} = 238$ Bit/s and $QBER_{9ns} = 11.34\%$, $SKR_{9ns} = 414$ Bit/s, respectively. Below 3 ns filtering, the SKR becomes significantly low, making it inefficient for any practical purposes. On the other hand, extending the temporal filtering duration increases the SKR but also brings the QBER closer to insecure limits.[48] Performance optimization via similar temporal filtering process was also reported for QD-based QKD systems recently.[49] It is important to highlight that the measured key rate is limited by the maximum available power of the excitation laser. As we discussed earlier, the SKR is expected to be at least a factor of 3 higher under stronger excitation conditions.

To give an idea about the capacity of our SPS, we simulate the secret key rate per pulse for a BB84-based QKD system using the experimentally measured values given above. The secret key rate is given by,[50]

$$R = \frac{P_{click}}{2}\{\beta\tau(QBER) - f(QBER)h(QBER)\} \quad (1)$$

The factor 1/2 is the efficiency of BB84 protocol and P_{click} is the detection probability of a signal at Bob's side. Equation (1) also contains multi-photon probability correction $\beta = (P_{click} - P_m)/P_{click}$, where $P_m = (1/2)\mu^2 g^2(0)$ is the multi-photon detection probability. Here, the expected QBER is given as

$$QBER = \frac{q\,P_{signal}}{P_{click}} + \frac{P_{dc}/2}{P_{click}} \quad (2)$$

where q is the error rate that comes from optical misalignment, P_{signal} is the probability of detecting a signal, and P_{dc} is the total probability of detecting dark count in a time window, which can

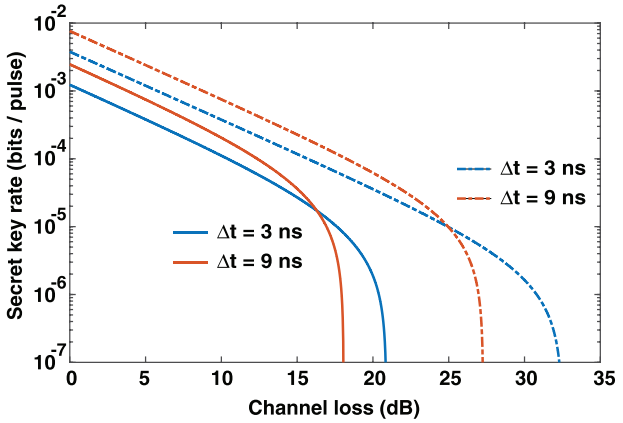

Figure 5. Secret key rate versus channel loss simulations for $\Delta t = 3$ *ns* and $\Delta t = 9$ *ns* values. Solid lines are obtained with the experimentally measured values while the dashed lines are calculated for an optimized experimental setup with better optical transmission and lower dark counts of APDs.

be written as the product of the dark count rate r_d and the temporal duration Δt ($P_{dc} = r_d\,\Delta t$). Finally, the function τ(QBER) is used as compression factor that accounts for the photon splitting attacks, f(QBER) represents the effect of the error correction process and h(QBER) is the well-known binary Shanon-entropy.[50] As given in Equations (1) and (2), the mean photon number of the source and the purity of the emission have a strong influence on the upper value of secret key rate, while the dark counts of detectors and the losses in the system limit the maximum distance for the useful secret key rate. In addition, applying a controlled amount of temporal filtering can improve the purity of the source and the QBER, therefore, extending the secret key rate for longer distances, as discussed earlier.

To quantify the effect of Δt, simulations are performed for two temporal filtering window values, results of which are shown in **Figure 5**. The solid lines represent the simulations for the measured parameters of the source and the existing experimental setup: $\mu = 0.0117$ (0.0234) and $g^2(0) = 0.046$ (0.080) for $\Delta t = 3$ *ns* (9 ns). Please note that the given mean photon number is measured right before the quantum channel, giving values comparable with the other state-of-the-art SPSs.[49,51] 35% transmission of the QKD setup (including optical losses, coupling into multi-mode fibers, and coupling to the APDs), and 70% quantum efficiency of the APDs with a dark count of 1.5 kHz are considered in our simulations. Summary of important parameters and the results of QKD experiment discussed above are given in **Table 1**. Finally, to evaluate the performance of our SPS, simulations are repeated for an optimized setup. A direct coupling of single photon emission to the QKD system without a PM fiber in Alice will lead almost a factor of 2 enhancement in mean photon number. In addition, removing the multimode fibers and replacing the APDs with the ones that have lower dark counts (25 Hz) will enhance the optical transmission and secret key rate with a lower QBER. Dashed lines in Figure 5 show the results for $\mu = 0.023$ (0.046) for the optimized setup and same $g^2(0)$ values as before under $\Delta t = 3$ *ns* (9 ns) conditions. As observed, using the same emitter studied here with cost-friendly and practical single photon detectors, almost a factor of four enhancement in secret key rate for a longer distance can be achieved.

Table 1. Results of QKD experiment under 1 MHz of operation at full excitation power of the source.

Δt (ns)	μ	$g^2(0)$	SKR (Bit/s)	QBER (%)
3	0.0117	0.046	238	8.95
9	0.0234	0.080	414	11.34

4. Conclusion

In conclusion, we have presented, to the best of our knowledge, the first demonstration of QKD with single photons generated from defects in hBN at room temperature. Due to the limited bandwidth of high-voltage amplifier driving the electro-optical modulator, the QKD experiment is operated at 1 MHz, which results in a sifted key rate of 238 bps and a QBER of 8.95%. The key rate can easily be increased up to tens of kHz by using a high-speed voltage amplifier or using a resonant modulator that can operate at a much lower driving voltage and consequently with high speed. Note that, the results presented in this work are obtained from a typical defect in hBN without applying any special technique or using any special components, such as higher NA microscope objective to enhance the collection efficiency. Brightness of these emitters can be improved via coupling to plasmonic antennas or cavity-based structures.[52,53] A recent study shows that utilization of commercially available solid immersion lenses (SIL) on hBN enhances both the excitation and photon collection efficiencies without the need of precise positioning of the SIL.[45] In addition, single photon purity of the source can be improved strongly by coupling the emitters to photonic cavities that suppress the off-resonant noise in the emission spectrum[54] or by temporal filtering of multi-photon emission processes using amplitude modulation techniques.[55] As a final note, because of its wide band gap, hBN hosts several types of defects with bright and sharp ZPL emission over a wide spectral range from UV to NIR.[34,56] It might be possible to find a defect emitting at high-transmission window needed for a low-loss free-space communication. According to the results presented here together with the possible improvements mentioned above, we believe that defects in hBN have a great potential for practical implementation of high-speed and long distance free-space QKD.

Note: We are aware of a recent report on an emulation of QKD with single photon emission from a monolayer TMDC material at cryogenic temperature.[57]

Acknowledgements

This work was supported by the Scientific and Technological Research Council of Turkey (TUBITAK) grant nos. 117F495 and 116F188. The authors thank Tobias Heindel for the fruitful discussions during the preparation of the manuscript. S.A. acknowledges the support from TUBITAK-BILGEM for providing equipment and the support from Turkish Academy of Sciences (TUBA-GEBIP).

Conflict of Interest

The authors declare no conflict of interest.

Data Availability Statement

The data that support the findings of this study are available from the corresponding author upon reasonable request.

Keywords

B92 protocol, defects, hexagonal boron nitride, quantum communication, quantum key distribution, single photon sources

Received: June 13, 2022
Revised: July 13, 2022
Published online: August 3, 2022

[1] C. H. Bennett, G. Brassard, in *Advances in Cryptology* (Eds: G. R. Blakley, D. Chaum), Springer Berlin Heidelberg, Berlin **1985**, pp. 475–480.
[2] C. H. Bennett, F. Bessette, G. Brassard, L. Salvail, J. Smolin, *J. Cryptol.* **1992**, *5*, 3.
[3] G. Brassard, N. Lütkenhaus, T. Mor, B. C. Sanders, *Phys. Rev. Lett.* **2000**, *85*, 1330.
[4] W.-Y. Hwang, *Phys. Rev. Lett.* **2003**, *91*, 057901.
[5] H.-K. Lo, X. Ma, K. Chen, *Phys. Rev. Lett.* **2005**, *94*, 230504.
[6] J. Wang, F. Sciarrino, A. Laing, M. G. Thompson, *Nat. Photonics* **2020**, *14*, 273.
[7] T. K. Paraïso, T. Roger, D. G. Marangon, I. D. Marco, M. Sanzaro, R. I. Woodward, J. F. Dynes, Z. Yuan, A. J. Shields, *Nat. Photonics* **2021**, *15*, 850.
[8] E. Waks, K. Inoue, C. Santori, D. Fattal, J. Vuckovic, G. S. Solomon, Y. Yamamoto, *Nature* **2002**, *420*, 762.
[9] P. M. Intallura, M. B. Ward, O. Z. Karimov, Z. L. Yuan, P. See, A. J. Shields, P. Atkinson, D. A. Ritchie, *Appl. Phys. Lett.* **2007**, *91*, 161103.
[10] R. J. Collins, P. J. Clarke, V. Fernández, K. J. Gordon, M. N. Makhonin, J. A. Timpson, A. Tahraoui, M. Hopkinson, A. M. Fox, M. S. Skolnick, G. S. Buller, *J. Appl. Phys.* **2010**, *107*, 073102.
[11] K. Takemoto, Y. Nambu, T. Miyazawa, K. Wakui, S. Hirose, T. Usuki, M. Takatsu, N. Yokoyama, K. Yoshino, A. Tomita, S. Yorozu, Y. Sakuma, Y. Arakawa, *Appl. Phys. Express* **2010**, *3*, 092802.
[12] T. Heindel, C. A. Kessler, M. Rau, C. Schneider, M. Fürst, F. Hargart, W.-M. Schulz, M. Eichfelder, R. Roßbach, S. Nauerth, M. Lermer, H. Weier, M. Jetter, M. Kamp, S. Reitzenstein, S. Höfling, P. Michler, H. Weinfurter, A. Forchel, *New J. Phys.* **2012**, *14*, 083001.
[13] M. Rau, T. Heindel, S. Unsleber, T. Braun, J. Fischer, S. Frick, S. Nauerth, C. Schneider, G. Vest, S. Reitzenstein, M. Kamp, A. Forchel, S. Höfling, H. Weinfurter, *New J. Phys.* **2014**, *16*, 043003.
[14] A. Beveratos, R. Brouri, T. Gacoin, A. Villing, J.-P. Poizat, P. Grangier, *Phys. Rev. Lett.* **2002**, *89*, 187901.
[15] R. Alléaume, F. Treussart, G. Messin, Y. Dumeige, J.-F. Roch, A. Beveratos, R. Brouri-Tualle, J.-P. Poizat, P. Grangier, *New J. Phys.* **2004**, *6*, 92.
[16] M. Leifgen, T. Schröder, F. Gädeke, R. Riemann, V. Métillon, E. Neu, C. Hepp, C. Arend, C. Becher, K. Lauritsen, O. Benson, *New J. Phys.* **2014**, *16*, 023021.
[17] M. K. Bhaskar, R. Riedinger, B. Machielse, D. S. Levonian, C. T. Nguyen, E. N. Knall, H. Park, D. Englund, M. Lončar, D. D. Sukachev, M. D. Lukin, *Nature* **2020**, *580*, 60.
[18] G. Murtaza, M. Colautti, M. Hilke, P. Lombardi, F. S. Cataliotti, A. Zavatta, D. Bacco, C. Toninelli, *arXiv:2202.12635* **2022**.
[19] A. K. Ekert, *Phys. Rev. Lett.* **1991**, *67*, 661.
[20] C. H. Bennett, G. Brassard, N. D. Mermin, *Phys. Rev. Lett.* **1992**, *68*, 557.
[21] T. Jennewein, C. Simon, G. Weihs, H. Weinfurter, A. Zeilinger, *Phys. Rev. Lett.* **2000**, *84*, 4729.
[22] B. Dzurnak, R. M. Stevenson, J. Nilsson, J. F. Dynes, Z. L. Yuan, J. Skiba-Szymanska, I. Farrer, D. A. Ritchie, A. J. Shields, *Appl. Phys. Lett.* **2015**, *107*, 261101.
[23] C. Schimpf, M. Reindl, D. Huber, B. Lehner, S. F. C. D. Silva, S. Manna, M. Vyvlecka, P. Walther, A. Rastelli, *Sci. Adv.* **2021**, *7*, eabe8905.
[24] F. B. Basset, M. Valeri, E. Roccia, V. Muredda, D. Poderini, J. Neuwirth, N. Spagnolo, M. B. Rota, G. Carvacho, F. Sciarrino, R. Trotta, *Sci. Adv.* **2021**, *7*, eabe6379.
[25] M. Kianinia, Z.-Q. Xu, M. Toth, I. Aharonovich, *Appl. Phys. Rev.* **2022**, *9*, 011306.
[26] G. Cassabois, P. Valvin, B. Gil, *Nat. Photonics* **2016**, *10*, 262.
[27] L. Weston, D. Wickramaratne, M. Mackoit, A. Alkauskas, C. G. V. d. Walle, *Phys. Rev. B* **2018**, *97*, 214104.
[28] T. T. Tran, K. Bray, M. J. Ford, M. Toth, I. Aharonovich, *Nat. Nanotechnol.* **2016**, *11*, 37.
[29] L. J. Martínez, T. Pelini, V. Waselowski, J. R. Maze, B. Gil, G. Cassabois, V. Jacques, *Phys. Rev. B* **2016**, *94*, 121405.
[30] G. Grosso, H. Moon, C. J. Ciccarino, J. Flick, N. Mendelson, L. Mennel, M. Toth, I. Aharonovich, P. Narang, D. R. Englund, *ACS Photonics* **2020**, *7*, 1410.
[31] N. R. Jungwirth, B. Calderon, Y. Ji, M. G. Spencer, M. E. Flatté, G. D. Fuchs, *Nano Lett.* **2016**, *16*, 6052.
[32] M. Kianinia, B. Regan, S. A. Tawfik, T. T. Tran, M. J. Ford, I. Aharonovich, M. Toth, *ACS Photonics* **2017**, *4*, 768.
[33] R. Bourrellier, S. Meuret, A. Tararan, O. Stéphan, M. Kociak, L. H. G. Tizei, A. Zobelli, *Nano Lett.* **2016**, *16*, 4317.
[34] T. T. Tran, C. Elbadawi, D. Totonjian, C. J. Lobo, G. Grosso, H. Moon, D. R. Englund, M. J. Ford, I. Aharonovich, M. Toth, *ACS Nano* **2016**, *10*, 7331.
[35] A. B. D.-a.-j.-w.-i. Shaik, P. Palla, *Sci. Rep.* **2021**, *11*, 12285.
[36] S. J. U. White, F. Klauck, T. T. Tran, N. Schmitt, M. Kianinia, A. Steinfurth, M. Heinrich, M. Toth, A. Szameit, I. Aharonovich, A. S. Solntsev, *J. Opt.* **2021**, *23*, 1.
[37] A. Kubanek, arXiv:2201.13184, **2022**.
[38] Y. Chen, T. N. Tran, N. M. H. Duong, C. Li, M. Toth, C. Bradac, I. Aharonovich, A. Solntsev, T. T. Tran, *ACS Appl. Mater. Interfaces* **2020**, *12*, 25464.
[39] T. Vogl, H. Knopf, M. Weissflog, P. K. Lam, F. Eilenberger, *Phys. Rev. Res.* **2021**, *3*, 013296.
[40] C. H. Bennett, *Phys. Rev. Lett.* **1992**, *68*, 3121.
[41] O. Ari, N. Polat, V. Fırat, Ö. Çakır, S. Ates, arXiv:1808.10611, **2018**.
[42] G. Grosso, H. Moon, B. Lienhard, S. Ali, D. K. Efetov, M. M. Furchi, P. Jarillo-Herrero, M. J. Ford, I. Aharonovich, D. Englund, *Nat. Commun.* **2017**, *8*, 705.
[43] N. R. Jungwirth, G. D. Fuchs, *Phys. Rev. Lett.* **2017**, *119*, 057401.
[44] N. Nikolay, N. Mendelson, E. Özelci, B. Sontheimer, F. Böhm, G. Kewes, M. Toth, I. Aharonovich, O. Benson, *Optica* **2019**, *6*, 1084.
[45] H. Z. J. Zeng, M. A. P. Ngyuen, X. Ai, A. Bennet, A. S. Solnstev, A. Laucht, A. Al-Juboori, M. Toth, R. P. Mildren, R. Malaney, I. Aharonovich, *Opt. Lett.* **2022**, *47*, 1673.
[46] J. E. Frooech, S. Kim, N. Mendelson, M. Kianinia, M. Toth, I. Aharonovich, *ACS Nano* **2020**, *14*, 7085.
[47] M. Nguyen, S. Kim, T. T. Tran, Z. Q. Xu, M. Kianinia, M. Toth, I. Aharonovich, *Nanoscale* **2018**, *10*, 2267.
[48] D. Bunandar, L. C. Govia, H. Krovi, D. Englund, *npj Quantum Inf.* **2020**, *6*, 104.
[49] T. Kupko, M. v. Helversen, L. Rickert, J.-H. Schulze, A. Strittmatter, M. Gschrey, S. Rodt, S. Reitzenstein, T. Heindel, *npj Quantum Inf.* **2020**, *6*, 29.
[50] E. Waks, C. Santori, Y. Yamamoto, *Phys. Rev. A: At., Mol., Opt. Phys.* **2002**, *66*, 7.
[51] K. Takemoto, Y. Nambu, T. Miyazawa, Y. Sakuma, T. Yamamoto, S. Yorozu, Y. Arakawa, *Sci. Rep.* **2015**, *5*, 4.

[52] T. T. Tran, D. Wang, Z.-Q. Xu, A. Yang, M. Toth, T. W. Odom, I. Aharonovich, *Nano Lett.* **2017**, *17*, 2634.
[53] S. Häußler, G. Bayer, R. Waltrich, N. Mendelson, C. Li, D. Hunger, I. Aharonovich, A. Kubanek, *Adv. Opt. Mater.* **2021**, *9*, 2002218.
[54] T. Vogl, R. Lecamwasam, B. C. Buchler, Y. Lu, P. K. Lam, *ACS Photonics* **2019**, *6*, 1955.
[55] S. Ates, I. Agha, A. Gulinatti, I. Rech, A. Badolato, K. Srinivasan, *Sci. Rep.* **2013**, *3*, 1397.
[56] R. Camphausen, L. Marini, S. A. Tawfik, T. T. Tran, M. J. Ford, S. Palomba, *APL Photonics* **2020**, *5*, 076103.
[57] T. Gao, M. V. Helversen, C. Anton-Solanas, C. Schneider, T. Heindel, arXiv:2204.06427, **2022**.